

# Quantum Wave Function Collapse for Procedural Content Generation

Raoul Heese, *Fraunhofer ITWM, Fraunhofer-Platz 1, 67663 Kaiserslautern, Germany*

*Abstract—Quantum computers exhibit an inherent randomness, so it seems natural to consider them for procedural content generation. In this work, a quantum version of the famous (classical) wave function collapse algorithm is proposed. This quantum wave function collapse algorithm is based on the idea that a quantum circuit can be prepared in such a way that it acts as a special-purpose random generator for content of a desired form. The proposed method is presented theoretically and investigated experimentally on simulators and IBM Quantum devices.*

Wave function collapse (WFC) is a powerful tool for procedural content generation (PCG) that is for example used in video games, as it can save significant development time by automating the creation of diverse and complicated game elements. However, it is not limited to video games, but also has applications in various other fields, including art and design, where the need for algorithmically generated content is widespread. Content in this context can therefore have a broad range of meanings: Images, 3D models, game levels, text, sound or a combination of these, to name just a few examples.

The WFC algorithm [1] is a non-backtracking, greedy constraint solving method [2], [3] that is able to generate complex patterns based on a set of input samples. It is known for its ability to create diverse and complex outputs that resemble the input samples while exhibiting novel combinations and variations. WFC employs two implementation strategies: the *simple tiled model* and the *overlapping model*, which share an identical algorithm core [4]. In the simple tiled model, tilesets are manually prescribed with predefined adjacency constraints, whereas the overlapping model automatically generates this information from a sample input.

In both strategies, the output is compartmentalized into segments and the possibilities for each segment are iteratively constrained until a unique solution is determined. The term “wave function collapse” is borrowed from quantum physics because of the conceptual similarity. The “wave function” refers to the set of potential states of the segments, whereas the “col-

lapse” occurs during the iterative process of narrowing down the possibilities.

Despite its name, WFC is a purely classical algorithm. But even if WFC has nothing to do with quantum physics beyond the terminology, the question arises as to whether quantum computers can still be used to execute a genuine quantum version of the algorithm. The motivation for leveraging quantum computers for PCG, which is called quantum procedural content generation (QPCG) in the following, lies in their potential to introduce new levels of complexity, creativity, and efficiency. Because quantum physics exhibits intrinsic randomness [5], quantum random number generators (QRNGs) can be viewed as sources of true randomness [6], making them a natural choice for generating randomized content. In addition, quantum superposition allows the random generation of complex patterns and variations that classical algorithms might find challenging to generate efficiently.

Currently available noisy intermediate-scale quantum (NISQ) hardware has very limited capabilities and is subject to significant noise and uncertainty [7]. While these kind of disruptive effects are typically to be avoided, they can also lead to novel and unexpected results for the generated content, potentially fostering creativity. In this sense, despite the technological limitations, it seems promising to use quantum computers already today for simple PCG tasks and to study the results. For more complex tasks, hybrid quantum-classical algorithms are a promising strategy to overcome the limitations, for example by integrating quantum subroutines into classical PCG methods to increase variability and complexity.

QPCG is therefore a promising approach, currently mainly for research, but in the future possibly also for

© 2024 IEEE

Digital Object Identifier 10.1109/MCG.2024.3447775

practical applications. However, a general discussion of QPCG is beyond the scope of this paper. Instead, the focus will specifically be on the WFC algorithm and how it can be modified to enable the use of gate-based quantum computers [8]. This paper has four main contributions:

- A probabilistic formulation of the simple tiled model of WFC is presented as a foundation for a quantum version. We denote this formulation as classical wave function collapse (CWFC) to clearly distinguish between classical and non-classical approaches.
- The quantum wave function collapse (QWFC) method is proposed, which builds on the encoding of a probability distribution in a quantum circuit.
- The hybrid quantum-classical wave function collapse (HWFC) method is proposed to take into account the limitations of NISQ hardware.
- The proposed methods are tested on simulators and *IBM Quantum* devices.

The remainder of the manuscript is organized as follows. After a brief summary of related work, a formal description of CWFC is given in an appropriate probabilistic form, which subsequently allows the development of QWFC and HWFC. The proposed methods are then demonstrated in practice. Finally, the paper ends with a conclusion.

## RELATED WORK

There are many approaches to PCG, such as machine learning [9], evolutionary algorithms [10] and search-based methods [11]. WFC was originally proposed by Gumin [1] as an example of the latter. Subsequent research has extended the basic WFC algorithm to address its limitations and expand its capabilities [2], [3]. For example, by eliminating the need for two-dimensional grids [12], adding design constraints [13], or allowing interactive user control over the results [14], [15]. Better scaling and runtime can be achieved by a hierarchical approach [16], a nested approach [4] or by using bitwise operations [17].

In contrast to classical PCG, QPCG is much less common in the literature. Previous work on QPCG was mainly focusing on the quantum generalization of a blurring process [18], [19] and map generation using a quantum-enhanced decision making process [20]. Moreover, related projects have been carried out in connection with the development of quantum-inspired games [21].

## CLASSICAL METHODS

This section provides a formal framework for the following methods, referred to as probabilistic iterative PCG (PIPCG). Subsequently, it is shown how the common CWFC is a special case of PIPCG. Only the main features of PIPCG and CWFC are summarized, the technical details can be found in the appendix.

### Probabilistic Iterative PCG (PIPCG)

To begin with, it is first necessary to formally define the generated content at a sufficiently abstract level. For this purpose, it is presumed that any content instance  $C$  can be described as an ordered sequence of  $N$  segments

$$C := \{(1, v_1), \dots, (N, v_N)\} \in \mathcal{C}, \quad (1)$$

where each segment  $(i, v_i)$  is defined by a unique identifier  $i \in [1, N]$  and a value  $v_i \in A$  from an alphabet  $A := [1, W]$  consisting of  $W$  symbols with the notation  $[i, j] := \{i, \dots, j\}$ . The set of all possible content instances  $\mathcal{C}$  contains  $W^N$  elements. For example, if the content represents an image, its individual pixels can constitute the segments. Each pixel can attain one color from the available color space of the image (as its alphabet).

*Iterative Process.* The procedural generation of content instance  $C \in \mathcal{C}$  is realized through an iterative process, where each iteration  $k \in [1, N]$  consists of three steps:

- 1) Randomly select a new segment identifier  $s(k) \in [1, N]$  from a set of available identifiers with a user-defined probability distribution.
- 2) Randomly select a corresponding value  $v_{s(k)} \in A$  from a set of available values with a user-defined probability distribution.
- 3) Add the chosen segment  $(s(k), v_{s(k)})$  to the content instance.

By repeating these steps, the content instance is assembled in the sense of  $C(0) \xrightarrow{k=1} C(1) \xrightarrow{k=2} \dots \xrightarrow{k=N} C(N) \equiv C$ , where  $C(k) := \{(s(1), v_{s(1)}), \dots, (s(k), v_{s(k)})\}$  represents the generated partial content instance at the end of iteration  $k$ . After  $N$  iterations, the newly generated content instance is complete.

*Probabilistic Generation.* An essential concept of PCG is that only a limited subset of all possible content instances  $C \in \mathcal{C}$  is generated according to the designer's aesthetic preferences, a given set of rules, or some other underlying logic; otherwise, the instances could be drawn directly from  $\mathcal{C}$  with much less effort.

For PIPCG, the user-defined probability distributions for the segment identifiers and the corresponding values represent exactly this underlying logic.

Generating content with PIPCG effectively corresponds to drawing a sample from the random variable  $C \sim p(C)$ , where

$$p(C) = p(v_1, \dots, v_N) \quad (2)$$

denotes the probability to generate the content  $C$  in the form of Equation (1) with values  $v_1, \dots, v_N$ . Hence,  $\mathcal{C} := \{C \mid C \in \mathcal{C} \wedge p(C) > 0\}$  represents the set of all content instances that can potentially be generated out of all possible content instances  $\mathcal{C}$ .

### Classical Wave Function Collapse (CWFC)

CWFC can be understood as a special case of PIPCG. In this manuscript, only a simplified form of the simple tiled model of CWFC is considered (with the minor extension of graph-based adjacency [12]), as it is sufficient to capture the key components of the approach. To realize CWFC, the two randomized selection steps of PIPCG are chosen as follows:

- 1) For the segment identifier selection, the segments with the smallest Shannon entropy with respect to the available value options are chosen.
- 2) Value selection is determined by a pattern-based set of user-defined rules.

*Adjacency.* For the pattern-based value selection, the segments are organized in such a way that they have a predefined adjacency relationship to each other that does not change. For example, consider that the pixels of an image constitute the segments. Choosing adjacency between the nearest neighbors leads to an adjacency configuration with four directions (right, up, left, down) as shown in Figure 1.

Formally, each direction within a adjacency configuration is specified by an index  $d \in [1, D]$ , where  $D$  denotes the total number of directions. The direction-based adjacency relationship between different segments is then defined by the coefficients  $\alpha_{ij}^d \in \{0, 1\}$  for  $i, j \in [1, N]$  and  $d \in [1, D]$ . If  $\alpha_{ij}^d = 1$ , segment  $i$  is connected to segment  $j$  in direction  $d$ ; otherwise not. For each direction  $d$ , these coefficients form an adjacency matrix  $\alpha^d \in \{0, 1\}^{N \times N}$  of a directed graph with  $N$  vertices that represent the segments. Hence, the segment adjacency is in fact an abstract concept that is not necessarily related to the visual form of the content.

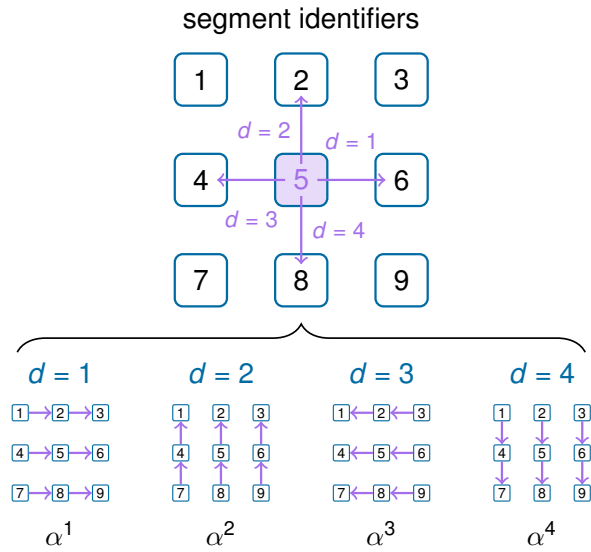


**FIGURE 1.** Exemplary nearest neighbor adjacency configuration for CWFC on a two-dimensional grid consisting of  $N = 9$  segments. The adjacency relationship for each of the four directions *right* ( $d = 1$ ), *up* ( $d = 2$ ), *left* ( $d = 3$ ), and *down* ( $d = 4$ ) can be represented as a directed graph with adjacency matrix  $\alpha^d$ .

*Patterns.* Patterns define how values are chosen based on the already generated content. A pattern

$$P := \{(d_1, v_1), \dots, (d_n, v_n)\} \quad (3)$$

consists of a set of  $n \leq D$  direction-value pairs with  $d_i \in [1, D]$  and  $v_i \in A$  for  $i \in [1, n]$ , which represents a layout of segments. A pattern-based rule

$$r_i^P(v, P, u) = (v, u, P) \quad (4)$$

is defined by a value  $v \in A$ , a factor  $u \in \mathbb{R}_{>0}$ , and a pattern  $P$ . It describes the weight  $u$  of selecting a value  $v$  for the target segment given the layout of adjacent segments  $P$ . The higher the value  $u$ , the more probable becomes the selection of the corresponding value. A selection mechanism with  $m$  rules is then fully defined by a ruleset

$$R := \{r_1, \dots, r_m\} \quad (5)$$

comprised of rules from Equation (4) with  $i \in [1, m]$ .

### CWFC Example: Checkerboard

As a simple example, consider the generation of images with black and white checkerboard patterns. The pixels of an image constitute the segments and the alphabet consists of only  $W = 2$  symbols standing for the

## FEATURE

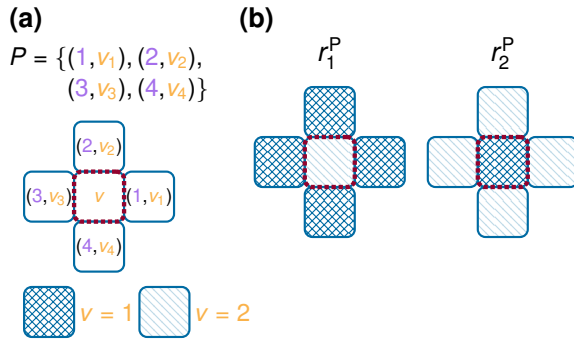


**FIGURE 2.** Visualization of pattern-based rules. (a) Visualization scheme. The center tile corresponds to the target segment  $i$  with a target value of  $v$ , whereas the adjacent tiles represent the required values  $v_1, \dots, v_4 \in \{1, 2\}$  of the four adjacent segments in the respective directions  $d = 1, \dots, d = 4$ . (b) Pattern-based rules  $r_1^P$  ( $v = 2, P = P_1, u = 1$ ) and  $r_2^P$  ( $v = 1, P = P_2, u = 1$ ), Equation (4), that can be used for the generation of images with black and white checkerboard patterns.

two colors. As an adjacency configuration, the nearest-neighbor adjacency from Figure 1 is presumed.

A checkerboard image can be achieved with only two patterns of the form of Equation (3), namely  $P_1 := \{(1, 1), (2, 1), (3, 1), (4, 1)\}$  and  $P_2 := \{(1, 2), (2, 2), (3, 2), (4, 2)\}$ . The corresponding ruleset, Equation (5), reads  $R = \{r_1^P, r_2^P\}$  and therefore contains the  $m = 2$  rules  $r_1^P$  ( $v = 2, P = P_1, u = 1$ ) and  $r_2^P$  ( $v = 1, P = P_1, u = 1$ ), see Figure 2.

The iterative process of CWFC is sketched in Figure 3 for a  $3 \times 3$  image (represented by  $N = 9$  segments). Only two content instances can be generated,  $C_1 := \{(1, 1), \dots\}$  and  $C_2 := \{(1, 2), \dots\}$  with equal probability  $p(C_1) = p(C_2) = \frac{1}{2}$ , Equation (2). The choice of the first value  $v_{s(1)}$  already determines the choices of all other values.

## QUANTUM METHODS

In the previous section, only classical PCG was considered. This section is about QPCG. First, QWFC is proposed as a special case of PIPCG. For this purpose, the probability distribution of the content instances  $p(C)$ , Equation (2), is realized with the help of a quantum circuit and the sampling is performed by exploiting the intrinsic randomness of quantum measurements. That is, the *actual* quantum mechanical wave function collapse is used to implement a quantum version of the Wave Function Collapse algorithm.

Subsequently, this section proposes HWFC as a

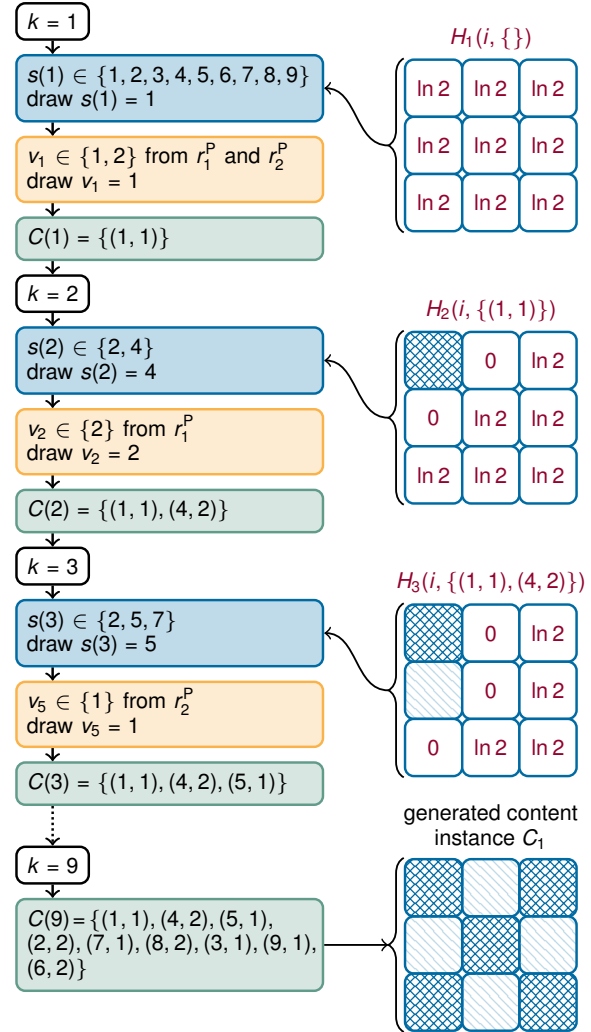


**FIGURE 3.** CWFC for the generation of  $3 \times 3$  images with checkerboard patterns defined by the rules from Figure 2. In each iteration  $k \in [1, 9]$ , three steps take place: (i) a segment identifier  $s(k)$  with the smallest entropy is drawn, (ii) a corresponding value  $v_{s(k)}$  is drawn according to the pattern-based ruleset, and (iii) the newly generated identifier-value pair is added as a segment to the content instance  $C(k)$ . For  $s(k)$  and  $v(k)$ , the uniformly distributed set of possible choices are listed. The choices for  $s(k)$  depend on the Shannon entropy  $H_k$  of each undefined segment (see appendix), as shown on the right. The choices for  $v(k)$  depend on the fulfillment of the two rules  $r_1^P$  and  $r_2^P$ , as listed.

quantum-classical hybrid algorithm based on content partitioning to overcome the limitations of NISQ devices. Only the main features of QWFC and HWFC are summarized, the technical details can be found in the appendix. A software implementation is available

online [22].

### Quantum Wave Function Collapse (QWFC)

To realize QWFC, the two randomized selection steps of PIPCG are chosen as follows:

- 1) The segment identifier selection is performed with a predefined order given by the vector  $\sigma \in S_N$ , where  $S_N$  is the set of all permutations of  $[1, N]$ .
- 2) The value selection is based on a pattern-based ruleset in the same way as for CWFC.

**Value Encoding.** The value for each segment is encoded by a set of qubits, which requires  $q := \lceil \log_2 W \rceil$  qubits for each segment  $i \in [1, N]$ . The group of  $q$  qubits that represent the value for segment  $i$  is denoted by  $Q_i := \{q_i^1, \dots, q_i^q\}$ , where  $q_i^j$  references the  $j$ 'th qubit of this group for  $j \in [1, q]$ . The state of these qubits encodes the value  $v_i$  of the segment  $i$  in binary as the tensor product sequence of qubit states  $\bigotimes_{j=1}^q |b_j\rangle = |v_i - 1\rangle_i \in \mathcal{H}_i$  via  $v_i - 1 = \sum_{j=1}^q b_j 2^{j-1}$  with  $b_j \in \{0, 1\}$ . Here,  $\mathcal{H}_i$  denotes the joint Hilbert space of all qubit from  $Q_i$  with  $v_i \in A$  for  $i \in [1, N]$ .

In total,  $Q := Nq$  qubits are required to represent the value of all  $N$  segments. The joint Hilbert space of all qubits from  $\bigcup_{i=1}^N Q_i$  is given by  $\mathcal{H} := \bigotimes_{i=1}^N \mathcal{H}_i$ .

**Probability Encoding.** Presume a state  $|\Psi\rangle \in \mathcal{H}$  that can realize samples from  $p(C)$ , Equation (2), with

$$p(C = \{(1, v_1), \dots, (N, v_N)\}) = |\langle \Psi | \bigotimes_{i=1}^N |v_i - 1\rangle_i|^2. \quad (6)$$

To prepare  $|\Psi\rangle$  from a ground state  $|0\rangle := \bigotimes_{i=1}^N |0\rangle_i$  based on a pattern-based ruleset  $R$ , Equation (5), a series of operators is applied, one for each iteration  $k \in [1, N]$  such that  $|\Psi\rangle := U_N \dots U_1 |0\rangle$  represents the final state after  $k$  iterations. In each iteration  $k$ , the state of the qubits  $Q_{\sigma_k}$  (that represent the value for segment  $\sigma_k$ ) is prepared conditioned on the state of (a subset of) the qubits  $Q_{\sigma_1}, \dots, Q_{\sigma_{k-1}}$  (that represent the values of the already prepared segments  $\sigma_1, \dots, \sigma_{k-1}$ ), which leads to an entangled joint state as sketched in Figure 4(a).

The required number of qubits for the proposed QWFC method increases linearly with the number of segments and logarithmically with the number of symbols in the alphabet. At the same time, the respective circuits may become exponentially deeper because of the costly conditional preparation of probability distributions [23].

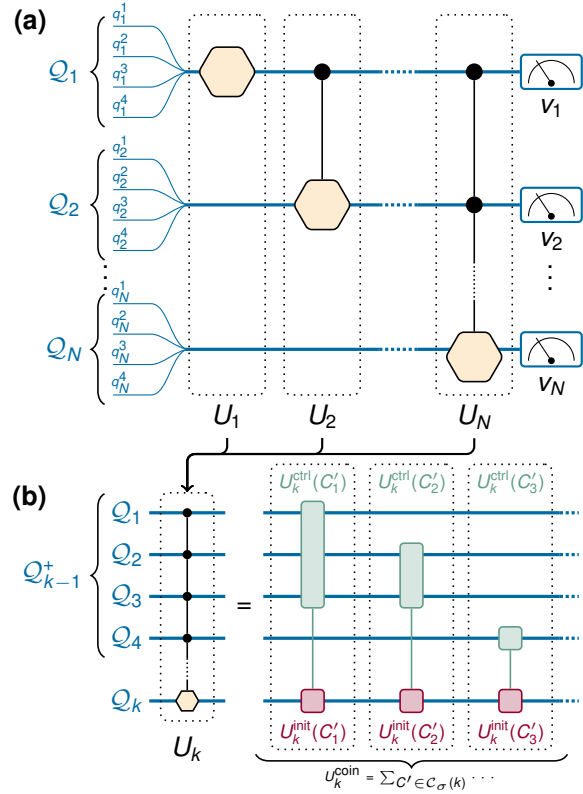


**FIGURE 4.** QWFC circuit with  $\sigma = (1, \dots, N)$ . (a) Circuit layout with an exemplary alphabet  $A$  with  $W = 16$  symbols, which requires a set  $Q_i$  of  $q = 4$  qubits for each segment with  $i \in [1, N]$ . In each iteration  $k \in [1, N]$ , the operator  $U_k$  prepares the qubits from  $Q_k$  in a superposition state  $|C'_k\rangle$ , entangled with (a subset of) the qubits from  $Q_1, \dots, Q_{k-1}$ . All qubits are measured to obtain  $p(C)$  (see appendix). (b) Gate decomposition of  $U_k$  into the components of  $U_k^{\text{coin}}$ , which consists of pairs  $U_k^{\text{ctrl}}(C'_k) \otimes U_k^{\text{init}}(C'_k)$ . Each of these pairs represent a conditional loading of a probability distribution. The combined control operators act on the qubits from  $Q_k^+$ , whereas the initialization operators act on the qubits from  $Q_k$  (see appendix).

### QWFC Example: Checkerboard

In the following, the above example for the generation of  $3 \times 3$  checkerboard images is considered for QWFC, where the predefined segment order  $\sigma = (1, 2, 3, 6, 5, 4, 7, 8, 9)$  is used as visualized in Figure 5(a). The resulting CWFC circuit is shown in Figure 5(b) and the resulting probability distribution of content instances  $p(C)$ , Equation (6), in Figure 5(c). A (noise-free) measurement of the circuit corresponds to drawing a sample from this distribution.

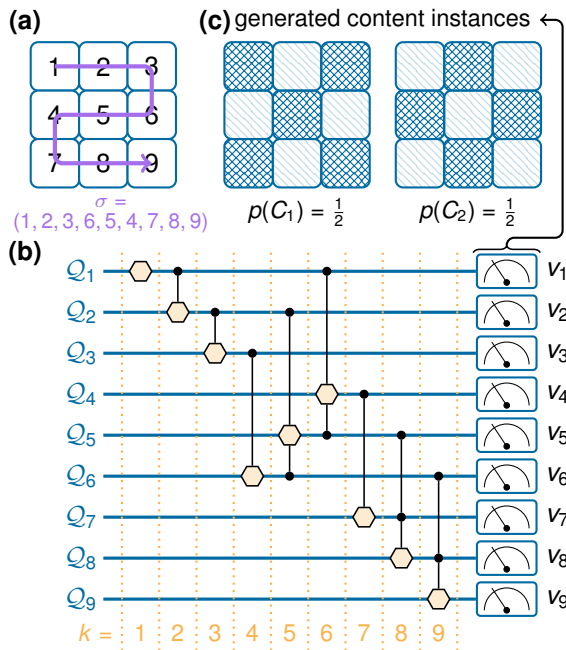


**FIGURE 5.** QWFC for the generation of  $3 \times 3$  images with black and white checkerboard patterns in analogy to Figure 3. (a) Predefined segment order  $\sigma = (1, 2, 3, 6, 5, 4, 7, 8, 9)$ . (b) Circuit layout with the same symbols as in Figure 4. (c) Generated content instances  $C_1$  and  $C_2$  with  $p(C_1) = p(C_2) = \frac{1}{2}$ .

### Hybrid Quantum-Classical WFC (HWFC)

HWFC represents a resource-efficient alternative to QWFC that might be more suitable for NISQ devices. The key idea of this approach is to separate the content into  $H$  partitions, each containing a subset of the segments as sketched in Figure 6. For each partition  $h \in [1, H]$ , a QWFC is performed, which yields the content instance partition  $C^h$  as a sample of the random variable  $C^h \sim p(C^h) := p^h(C^h | C^1, \dots, C^{h-1})$  in analogy to Equation (6). To apply QWFC on the partition, two modifications are required. First, the iteration over all segment identifiers  $[1, N]$  is replaced by the iteration over the segment identifiers from  $S^h$ . Second, the already sampled sub-contents  $C^1, \dots, C^{h-1}$  from the partitions  $[1, h-1]$  are used as an additional constraint for the pattern-based rules. This modification induces classical correlations from previously sampled content partitions into the circuit and therefore requires a *conditional* form of QWFC that respects these correlations as constraints. The resulting distribution of the joint content instances is then given by  $p(C = \bigcup_{h=1}^H C^h) = \prod_{h=1}^H p^h(C^h | C^1, \dots, C^{h-1})$  and requires less quantum resources than performing a single run of QWFC on all segments.

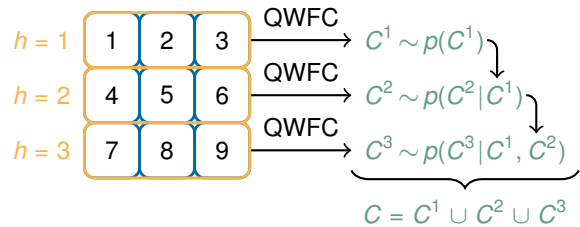


**FIGURE 6.** HWFC with  $H = 3$  partitions of  $N = 9$  segments. For each partition, a *conditional* QWFC is performed and the resulting content instances are combined.

## DEMONSTRATION

In the present section, five simple content creation use cases are presented to demonstrate the proposed methods. For QWFC and HWFC, both idealized (i.e., noise-free) simulators and *IBM Quantum* devices were used, the latter being accessed via the *IBM Quantum Cloud Services* [24] during December 2023.

### Checkerboard Revisited

The first use case is the previously presented checkerboard example, cf. Figures 2 and 5. Again,  $3 \times 3$  instances are considered, for which a comparison between QWFC and HWFC is performed on the *IBM Quantum* device *ibm\_kyoto* (Eagle r3 processor version 1.2.4, 127 qubits). For QWFC, 10 000 shots are measured, each yielding a content instance. For HWFC,  $H = 3$  equal-sized partitions are used in analogy to Figure 6 and the method is repeated 131 times, each time yielding a content instance. The results are shown in Figure 7.

In total, there are  $2^9 = 512$  possible content instances  $C \in \mathcal{C}$ , but only two of them,  $C_1$  and  $C_2$ , are valid. The remaining 510 content instances are invalid because they violate the prescribed patterns. In Figure 7(a), QWFC is able to generate the two valid instances, but at the same time also produces a lot of invalid instances due to hardware imperfections. From Figure 7(b) it can be seen that the results from HWFC are much closer to the idealized solution that would contain only  $C_1$  and  $C_2$  with equal probability. It is a consequence of the reduced circuit size from this method that invalid solutions occur with much less frequency than for QWFC.

### Pipes

The second use case is to create an image from tiles of seven different pipe (or line) sections as well as one blank tile. That is, the alphabet consists of

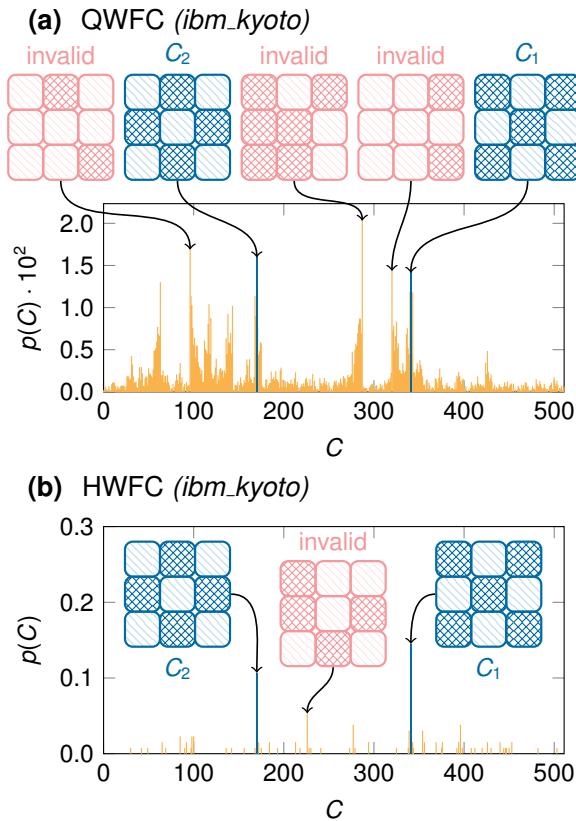


**FIGURE 7.** Checkerboard generation. Plots show the generated content instances  $C$ , Equation (1), (encoded as integers in  $[0, 511]$  from the measured bit strings) and their respective probabilities  $p(C)$ , Equation (6). (a) QWFC on the *IBM Quantum* device *ibm\_kyoto*. The dominating instances ( $p(C) > 1.4 \times 10^{-2}$ ) are highlighted. (b) HWFC with  $H = 3$  on the same device results in less invalid instances.

$W = 8$  symbols and each tile in the image constitutes a segment. The alphabet is shown in Figure 8(a). As adjacency configuration, the nearest-neighbor adjacency from Figure 1 is presumed with  $D = 4$ . The pattern-based ruleset is chosen in such a way that neighboring tiles have to form a connecting network of pipes. Three example rules for this purpose are shown in Figure 8(b). In total,  $m = 2048$  rules are required to achieve this goal.

Exemplarily, images consisting of  $10 \times 4$  tiles ( $N = 40$ ) are considered, for which a comparison between HWFC on the *IBM Quantum* device *ibm\_kolkata* (Falcon r5.11 processor version 1.14.8, 27 qubits), HWFC on a simulator and CWFC is performed. For HWFC,  $H = 10$  equal-sized partitions are used, each corresponding to one column of the image. A few resulting instances are shown in Figure 8(c).

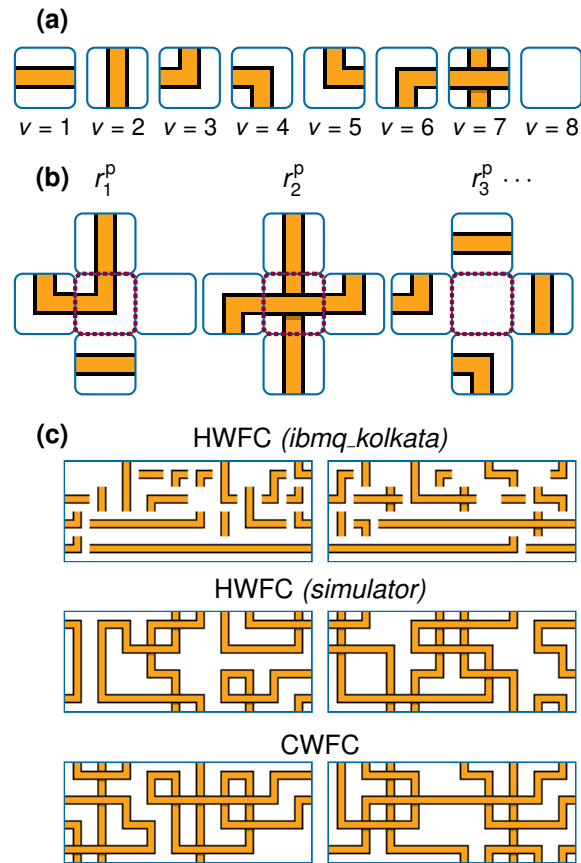


**FIGURE 8.** Pipe generation. The generated image is required to show a network of connected pipes. (a) Alphabet consisting of  $W = 8$  symbols, each of which represents a tile with a pipe section and an empty tile. (b) Example of three pattern-based rules  $r_1^p$ ,  $r_2^p$ , and  $r_3^p$ , cf. Figure 2. (c) Example  $10 \times 4$  tile images that were generated using HWFC with  $H = 10$  on the *IBM Quantum* device *ibm\_kolkata* and a simulator; also shown are images from CWFC.

Based on a visual comparison, both CWFC and HWFC on the simulator yield similar results, as expected. However, the results from *ibm\_kolkata* clearly contain a lot of invalid patterns as a result of the imperfect hardware. This demonstrates the limitations of the proposed method on NISQ devices.

### Hexagon Map

The third use case addresses images based on hexagonal tiles that can be interpreted as a map consisting of different terrains. For this purpose, an alphabet of  $W = 4$  symbols is chosen, each corresponding to a unicolored tile (blue, yellow, green, and gray) and each tile constitutes a segment. As adjacency configuration,

## FEATURE

a nearest-neighbor adjacency is presumed ( $D = 6$ ). The prescribed pattern-based ruleset only allows connections of the form blue-yellow-green-gray, which can be fulfilled with  $m = 1586$  rules, see Figure 9(a). To promote a higher occurrence of blue tiles, the factors in Equation (4) are chosen as  $u = 5$  for blue tiles and  $u = 1$  otherwise.

As a first example, images consisting of  $N = 7$  tiles are considered, for which QWFC on a simulator and CWFC are performed. The resulting distributions of content instances  $p(C)$  in Figure 9(b) is exactly calculated for QWFC, Equation (6), and based on 10 000 samples for CWFC, Equation (2). Both distributions are significantly different, which is no surprise since the two approaches use a different segment identifier selection. The second example considers images from  $N = 127$  tiles, for which HWFC with  $H = 20$  is performed on a simulator. Example instances are shown in Figure 9(c).

### Platformer

The fourth use case is motivated by computer game level design. The goal is to create a platformer-type level from a set of eight tiles [25], each corresponding to a different game element (ground, grass, mushroom, block, air, and a tree that is composed of three tiles). Consequently, the alphabet consists of  $W = 8$  symbols, see Figure 10(a). As adjacency configuration, the two tiles above and below are taken into account as neighbors ( $D = 2$ ). A pattern-based ruleset is prescribed that meets five requirements: (i) The bottom row consists of ground tiles and ground tiles can only be placed on top of each other, (ii) only a grass tile or a mushroom tile can be placed above a ground tile, (iii) tree tiles must be placed in order with the lowest tile above a grass tile, (iv) air tiles can only be placed above grass, mushroom or other air tiles, (v) block tiles can only be placed between two air tiles. These requirements can be fulfilled with  $m = 15$  rules, see Figure 10(b). The first requirement can be resolved with a functional factor  $u(i)$  in Equation (4) that vanishes for all non-ground tiles in the bottom row (see appendix). For all non-vanishing cases,  $u = 0.1$  for  $r_6^p$  and  $u = 1$  otherwise to reduce the occurrence of block tiles. The segment order  $\sigma$  is chosen such that the levels are built up from bottom to top.

Exemplarily, levels with  $10 \times 10$  tiles are considered, for which HWFC with  $H = 20$  equal-sized partitions (each corresponding to a half row of the level) is performed on a simulator. Four resulting instances are shown in Figure 10(c).

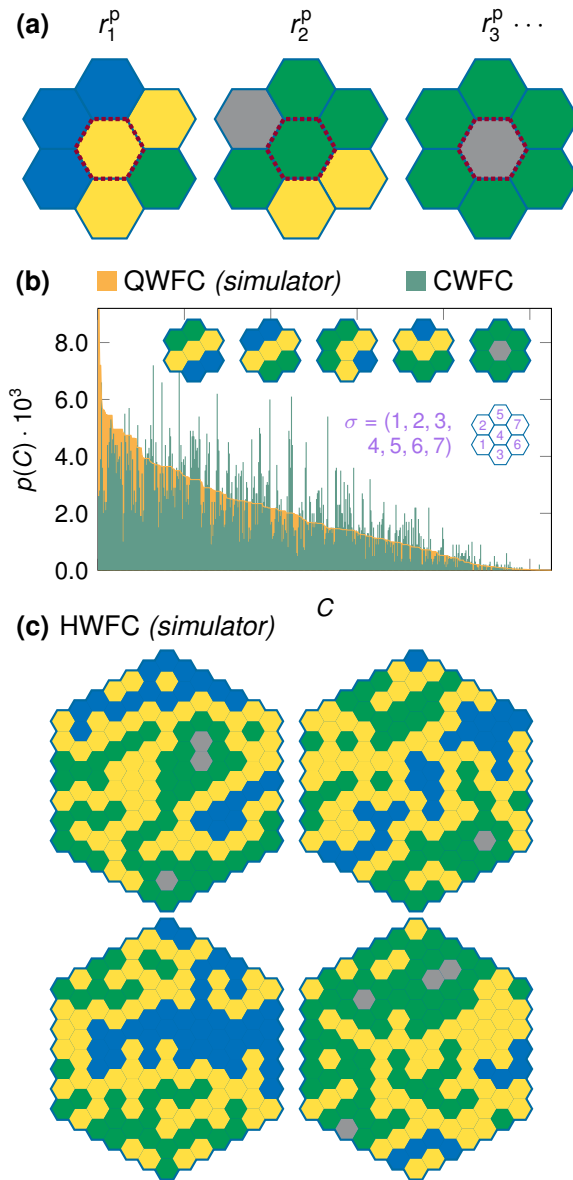


**FIGURE 9.** Map generation. Only connections of the form blue-yellow-green-gray are allowed. (a) Example of three pattern-based rules  $r_1^p$ ,  $r_2^p$ , and  $r_3^p$ . (b) Distribution of content instances  $p(C)$  for  $N = 7$  hexagons using QWFC on a simulator (sorted by descending probability) and CWFC (with the same ordering). The inset plot shows the predefined segment order  $\sigma$  and the five most probable instances for QWFC. The asymmetry is a consequence of the choice of  $\sigma$ . (c) Example images that were generated from  $N = 127$  hexagons using HWFC with  $H = 20$  on a simulator.

### Voxel Skyline

The final use case considers the creation of a three-dimensional voxel graphic with a binary alphabet of



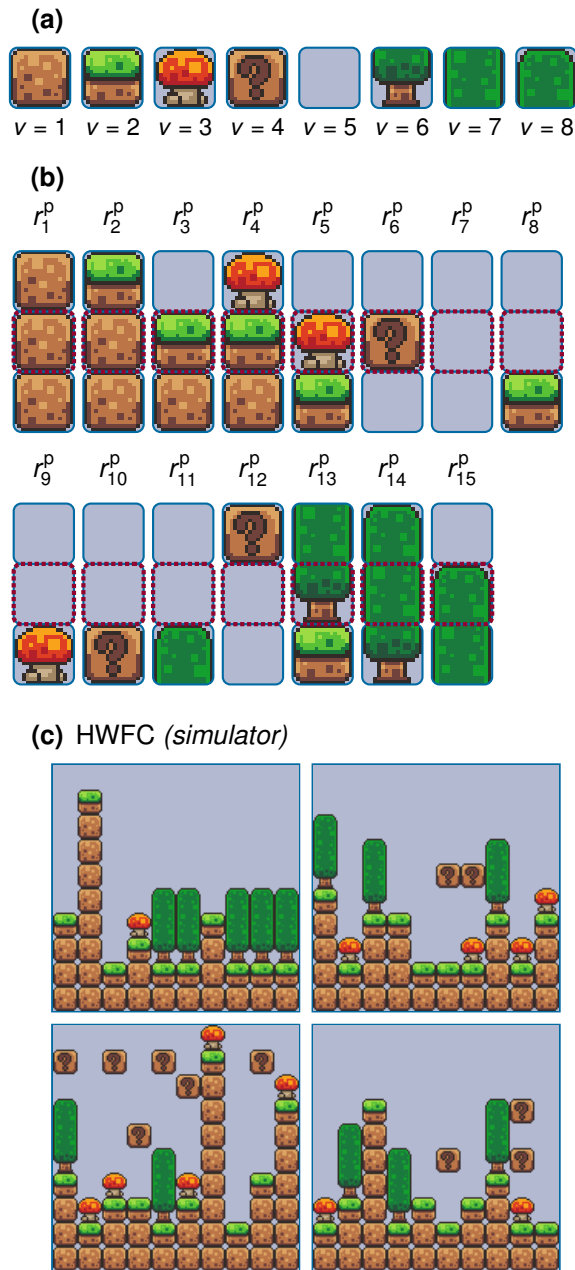


**FIGURE 10.** Level generation. (a) Alphabet consisting of  $W = 8$  symbols, each of which represents a tile [25]. (b) Pattern-based ruleset consisting of  $m = 15$  rules. (c) Example  $10 \times 10$  tile images that were generated using HWFC with  $H = 20$  on a simulator.

$W = 2$  symbols, which represent the presence or absence of a voxel. Each voxel constitutes a segment, as adjacency configuration the voxel above and below are taken into account ( $D = 2$ ). The chosen pattern-based ruleset with  $m = 4$  ensures that voxels are

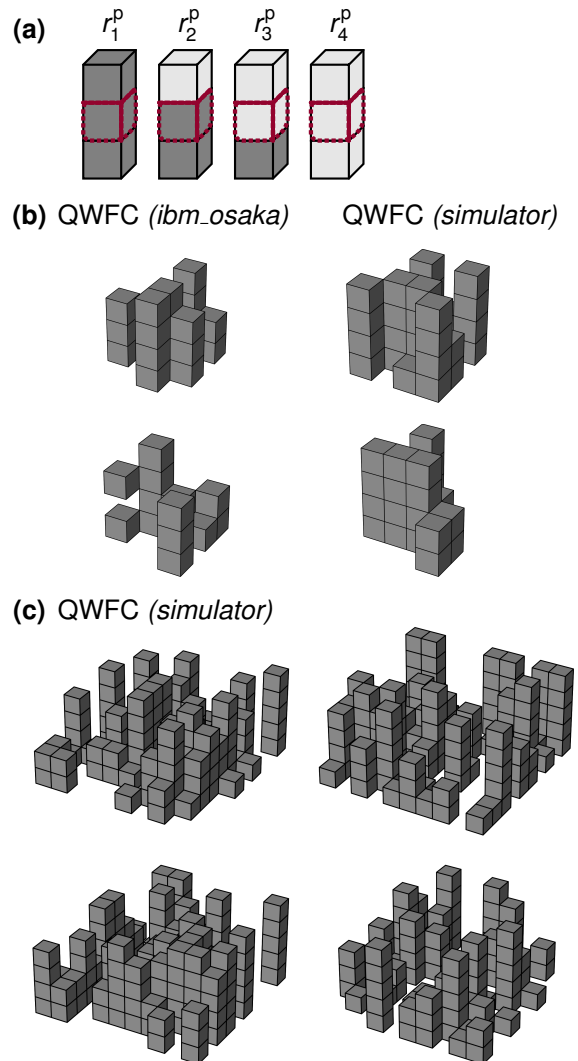


**FIGURE 11.** Skyline generation. (a) Pattern-based ruleset consisting of  $m = 4$  rules in an analogous representation as in the previous figures. (b) Example images from a  $4 \times 4 \times 4$  voxel grid that were generated using QWFC on the *IBM Quantum* device *ibm\_osaka* and a simulator. (c) Example images from a  $10 \times 10 \times 5$  voxel grid that were generated using QWFC on a simulator.

built from the ground up, see Figure 11(a). This leads to a skyline-like structure. Exemplarily, two cases are considered: First, images from a  $4 \times 4 \times 4$  voxel grid, for which QWFC is performed both on a the *IBM Quantum* device *ibm\_osaka* (Eagle r3 processor version 1.0.3, 127 qubits) and a simulator, see Figure 11(b). An error violating  $r_3^p$  can be seen in the bottom left image that results from hardware imperfections. Second, images

from a  $10 \times 10 \times 5$  voxel grid, for which QWFC is performed on a simulator, see Figure 11(c).

## CONCLUSION

In this work, QWFC was proposed as a method to realize WFC on a gate-based quantum computer as an example of QPCG. The idea is to construct a quantum circuit from which valid content instances (that fulfill the prescribed patterns) can be sampled via measurements. In other words, the quantum circuit acts as a special-purpose QRNG for content of a desired form that makes use of the intrinsic randomness of quantum physics. This means that the actual quantum mechanical collapse of the wave function is used for the implementation, from which the classical method derived its name.

The proposed method is not without its challenges. The generating quantum circuit becomes larger from both the content and alphabet size and at the same time deeper from correlations within the content instance distribution, which makes it difficult to evaluate practical use cases on current hardware. For this reason, HWFC was proposed as a hybrid method that partitions the generation into smaller tasks for QWFC.

The experimental results have shown the limitations of QWFC and HWFC, but have also proven that at least simple examples can already be implemented on today's quantum hardware. The biggest bottleneck of the circuit complexity is the conditional preparation of probability distributions. Investigating possible improvements in this area with regard to specific QPCG use cases could therefore be a potential direction for future research.

The conceptual advantage of QWFC is that a circuit, once designed, represents the distribution of content instances such that new instances can be generated by simple measurements without any additional algorithmic effort. A shortcoming of QWFC is that only a fixed order of segments is considered instead of a dynamic (e.g., entropy-based) order that depends on the previously selected segments, which is a chance for future improvements.

In conclusion, the paper aims to provide an initial approach to QPCG that demonstrates its feasibility but leaves room for improvement and raises the question of useful application areas given the limits of NISQ devices.

## APPENDIX

This appendix section contains the technical details of the presented PCG methods.

## Technical Details of PIPCG

Presume the generated partial content instance  $C(k) \in \mathcal{C}(k)$  for  $k \in [1, M]$ , where  $\mathcal{C}(k)$  denotes all possible partial content instances at the end of iteration  $k$  with  $\mathcal{C}(N) \equiv \mathcal{C}$ . One has  $|\mathcal{C}(k)| = k$ ,  $\mathcal{C}(k) = \mathcal{C}(k-1) \cup \{(s(k), v_{s(k)})\}$ ,  $s(i) \neq s(j) \forall i, j \in [1, k] \wedge i \neq j$ , and  $|\mathcal{C}(k)| = \sum_{l \in \mathcal{J}(k)} W^{|l|}$ , where  $\mathcal{J}(k) := \{l \mid l \in [1, M] \wedge |l| = k\}$  with  $|\mathcal{J}(k)| = \binom{M}{k}$ . Let  $\mathcal{C}(0) := \{\}$  and  $\mathcal{C}(0) := \{\mathcal{C}(0)\}$ . Furthermore,  $\mathcal{S}^+(\mathcal{C}(l)) := \{s(1), \dots, s(l)\}$  with  $|\mathcal{S}^+(\mathcal{C}(l))| = l$  and  $\mathcal{S}^-(\mathcal{C}(l)) := [1, M] \setminus \mathcal{S}^+(\mathcal{C}(l))$  with  $|\mathcal{S}^-(\mathcal{C}(l))| = M - l$  for all  $\mathcal{C}(l) \in \mathcal{C}(l)$  and for all  $l \in [0, M]$ .

In the following, the three steps within each iteration  $k$  of PIPCG are explained. In the first step, an identifier is selected by drawing a sample  $s(k)$  from the random variable

$$s(k) \sim p_k^s(i = s(k) \mid \mathcal{C}' = \mathcal{C}(k-1)). \quad (7)$$

The probability distribution  $p_k^s(i \mid \mathcal{C}')$  with support  $i \in [1, M]$  and  $\mathcal{C}' \in \mathcal{C}(k-1)$  is a user-defined parameter of the procedure that determines how new segment indices  $k$  are selected based on the partial content instance  $\mathcal{C}' = \mathcal{C}(k-1)$  that has already been generated up to the previous iteration  $k-1$  (making PIPCG non-Markovian). Two conditions must hold:

- S1) No identifier can be chosen twice, i.e.,  $p_k^s(i = s \mid \mathcal{C}' = \mathcal{C}(l-1)) = 0 \forall s \in \mathcal{S}^+(\mathcal{C}(l-1)) \forall \mathcal{C}(l-1) \in \mathcal{C}(l-1) \forall l \in [1, M]$ .
- S2) At least one valid identifier has to be available, i.e.,  $\forall l \in [1, M] \forall \mathcal{C}(l-1) \in \mathcal{C}(l-1) \exists s \in \mathcal{S}^-(\mathcal{C}(l-1)) : p_k^s(i = s \mid \mathcal{C}' = \mathcal{C}(l-1)) > 0$ .

In the second step, a value  $v_{s(k)}$  is selected for the segment by drawing a sample  $v_{s(k)}$  from the random variable

$$v_{s(k)} \sim p_k^v(\nu = v_{s(k)} \mid i = s(k), \mathcal{C}' = \mathcal{C}(k-1)). \quad (8)$$

The probability distribution  $p_k^v(\nu \mid i, \mathcal{C}')$  with support  $\nu \in A$ ,  $i \in [1, M]$  and  $\mathcal{C}' \in \mathcal{C}(k-1)$  is a user-defined parameter of the procedure that determines how new values are selected based on the selected identifier  $i = s(k)$  of the current iteration and  $\mathcal{C}' = \mathcal{C}(k-1)$ . Two conditions must hold:

- V1) Only values from the alphabet are available, i.e.,  $p_k^v(\nu = v \mid i = s, \mathcal{C}' = \mathcal{C}(l)) = 0 \forall v \notin A \forall s \in [1, M] \forall \mathcal{C}(l) \in \mathcal{C}(l-1) \forall l \in [1, M]$ .
- V2) At least one value from the alphabet has to be available, i.e.,  $\forall l \in [1, M] \forall \mathcal{C}(l-1) \in \mathcal{C}(l-1) \forall s \in \mathcal{S}^-(\mathcal{C}(l-1)) \exists v \in A : p_k^v(\nu = v \mid i = s, \mathcal{C}' = \mathcal{C}(l)) > 0$ .

In the third step,  $\mathcal{C}(k) = \mathcal{C}(k-1) \cup \{(s(k), v_{s(k)})\}$ . The process is repeated for  $k \rightarrow k+1$  until  $k = N$ .

The probability to generate  $C(k)$  is given by  $p(C(k)) := \sum_{\sigma \in S_k(C(k))} \prod_{l=1}^k q_l^k(\sigma, C(k))$ , where

$$q_l^k(\sigma, C(k)) := p_l(i = \sigma_l, \nu = v_{\sigma_l})$$

$$C' = \{(\sigma_1, v_{\sigma_1}), \dots, (\sigma_{l-1}, v_{\sigma_{l-1}})\}. \quad (9)$$

with  $p_l(i, \nu | C') := p_k^s(i | C') p_k^v(\nu | i, C')$ ,  $S_k(C(k))$  as the set of all permutations of  $S^+(C(k))$  with  $|S_k(C(k))| = k!$ , and the  $l$ th value of a permutation  $\sigma \in S_k(C(k))$  denoted by  $\sigma_l$  for  $l \in [1, k]$ . In Equation (9), let  $C' = \{\}$  for  $l = 1$ .  $v_{\sigma_m}$  represents the value of the segment with identifier  $\sigma_m$  from the content instance  $C(k)$  for  $m \in [1, l]$ . The support  $\underline{C}(k) := \{C(k) | C(k) \in \mathcal{C}(k) \wedge p(C(k)) > 0\}$  of  $p(C(k))$  contains all  $C(k)$  that can be generated for the given  $k$ . For  $k = N$ , Equation (2) emerges with  $p(v_1, \dots, v_N) := \sum_{\sigma \in S_N} \prod_{l=1}^N q_l^N(\sigma, C)$  and  $\underline{C}(N) = \underline{C}$ .

### Technical Details of CWFC

For the value selection, a general rule-based selection mechanism is introduced first and then the pattern-based selection is presented as a special case. Consider a set of  $m$  rules  $R \in \mathcal{R}$ , Equation (5), with the set of all possible rulesets  $\mathcal{R}$ . Each rule  $r_i := r_i(v, w) := (v, w)$  for  $i \in [1, m]$  consists of a value  $v \in A$  and a weight function  $w := w(i, \alpha^d, C') \in \mathbb{R}_{\geq 0}$  with  $w : [1, M] \times \mathcal{B} \times \bar{\mathcal{C}} \rightarrow \mathbb{R}_{\geq 0}$ , where  $\bar{\mathcal{C}} := \cup_{k=0}^{N-1} \mathcal{C}(k)$  and  $\mathcal{B} := \{0, 1\}^{N \times N}$ . Given  $R \in \mathcal{R}$ ,  $p_k^v(\nu | i, C') = p_k^{v,R}(\nu | i, C') := \frac{F_k(\nu, i, C')}{\bar{F}_k(i, C')}$ , Equation (8), with  $F_k(\nu, i, C') := \sum_{(v, w) \in R} w(i, \alpha^d, C')$  and  $\bar{F}_k(i, C') := \sum_{\nu \in A} F_k(\nu, i, C')$  for  $\nu \in A$ ,  $i \in [1, M]$ ,  $C' \in \mathcal{C}(k)$  for  $k \in [1, M]$ , and  $\alpha^d \in \mathcal{B}$  for  $d \in [1, D]$ . Condition V1 is always satisfied, whereas in case of  $\bar{F}_k(i, C') \stackrel{!}{=} 0$  for any  $C' \in \mathcal{C}(k)$  with  $p_k^{s,H}(i | C') p(C') > 0$ , condition V2 is violated.

Pattern-based value selection is a special case of rule-based value selection, where  $w(i, \alpha^d, C') := w^P(i, \alpha^d, C', P, u) := u \tau(i, \alpha^d, C', P)$  of each rule  $r_i := r_i^P(v, P, u) := (v, w^P(i, \alpha^d, C', P, u))$  for  $i \in [1, m]$  is defined by  $u \in \mathbb{R}_{> 0}$  and  $P \in \mathcal{P}$ , Equation (3) with  $d_i \in [1, D]$  for  $i \in [1, n]$ ,  $d_i \neq d_j \forall i, j \in [1, n] \wedge i \neq j$ , and  $v_i \in A$  for  $i \in [1, n]$ . The set of all possible patterns reads  $\mathcal{P} := \{P | P \in ([1, D] \times A)^n \forall n \in [0, D]\}$ . A pattern  $P$  is fulfilled, if  $\tau(i, \alpha^d, C', P) := \prod_{(d, v) \in P} \prod_{(s, v') \in C' \wedge \alpha_{i, s}^d = 1} \delta_{v, v'} \in [0, 1]$  evaluates to one. The set of all possible pattern-based rulesets is denoted by  $\mathcal{R}^P \subset \mathcal{R}$ . Summarized, the weight function  $w(i, \alpha^d, C')$ , yields  $u$  if the pattern  $P$  applies and zero otherwise. Only adjacent segments (i.e.,  $\alpha_{i, s}^d = 1$ ) have an influence on  $p_k^v(\nu | i, C')$ .

The rules  $r_i$  can be rewritten in form of Equation (4). One has  $p_k^{v,R}(\nu | i, C') = p_k^{v,P}(\nu | i, C') := \sum_{(v, u, P) \in R} \gamma(u, i, C') \tau(i, \alpha^d, C', P)$  with  $\gamma(u, i, C') := \frac{u}{\bar{F}_k(i, C')} \in [0, 1]$ . Optionally, a functional factor instead

of a constant factor can be used, i.e.,  $u := u(i, C) : [1, M] \times \bar{\mathcal{C}} \rightarrow \mathbb{R}$ .

For the entropic segment identifier selection, one has

$$p_k^s(i | C') = p_k^{s,H}(i | C') := \begin{cases} |I_k(C')|^{-1} & \text{if } i \in I_k(C') \\ 0 & \text{otherwise} \end{cases} \quad (10)$$

in Equation (7) with  $I_k(C') := \{i | i \in S^-(C') \wedge H_k(i, C') = h_k(C')\}$  and  $h_k(C') := \arg \min_{j \in S^-(C')} H_k(j, C')$ , where  $H_k(i, C') := - \sum_{\nu \in A} p_k^{v,P}(\nu = v | i, C') \ln p_k^{v,P}(\nu = v | i, C')$  denotes the Shannon information entropy for  $C' \in \mathcal{C}(k-1)$ ,  $k \in [1, M]$ .

### Technical Details of QWFC

Presume a predefined order of segment indices  $\sigma \in S_N$ . Hence,  $p_k^s(i | C') = p_k^{s,0}(i | C') := \delta_{i, \sigma_i}$  and  $\mathcal{C}(k) = \mathcal{C}_\sigma(k) := \{C | C = \{(\sigma_1, v_{\sigma_1}), \dots, (\sigma_k, v_{\sigma_k})\} \forall v_{\sigma_l} \in A \forall l \in [1, k]\}$  for  $k \in [1, M]$  and  $\mathcal{C}_\sigma(0) := \{\{\}\}$ .

The value selection is pattern-based in analogy to CWFC, which together with the identifier selection leads to Equation (6). Given  $\sigma$  and  $R \in \mathcal{R}^P$ , the task is to prepare  $|\Psi\rangle$  from Equation (6) constructively with quantum gates. Let  $|\Psi\rangle := U_N \dots U_1 |0\rangle$  as in Figure 4(a). Then,

$$U_k := [U_k^{\text{coin}} + U_k^0] \otimes \bigotimes_{l=k+1}^N \mathbb{1}_{\sigma_l} \in \mathcal{H} \quad (11)$$

for  $k \in [1, M]$ , which contains  $\mathbb{1}_i \in \mathcal{H}_i$ , the unit operator for  $i \in [1, M]$  and two other operators.

First, the conditional initialization operator

$$U_k^{\text{coin}} = \sum_{C' \in \mathcal{C}_\sigma(k)} [U_k^{\text{ctrl}}(C') \otimes U_k^{\text{init}}(C')], \quad (12)$$

where  $U_k^{\text{ctrl}}(C') := \bigotimes_{(s, v) \in L_k(C')} |v-1\rangle \langle v-1|_s \in \bigotimes_{l=1}^{k-1} \mathcal{H}_{\sigma_l}$  denotes the control operator, and  $U_k^{\text{init}}(C') := |C'\rangle \langle 0|_{\sigma_k} \in \mathcal{H}_{\sigma_k}$  the initialization operator with  $|C'\rangle_{\sigma_k} := \sum_{\nu \in A} \sqrt{p_k^{v,P}(\nu | \sigma_k, C')} |\nu-1\rangle_{\sigma_k} \in \mathcal{H}_{\sigma_k}$ . The summation in  $U_k^{\text{ctrl}}(C')$  runs over all adjacent segments  $L_k(C') := \{(s, v) | (s, v) \in C' \wedge \exists P \in R_P \exists d \in P_d : \alpha_{\sigma_k, s}^d = 1\} \subseteq C'$ , where  $R_P := \{P_1, \dots, P_m\}$  stands for the set of patterns in  $R \in \mathcal{R}^P$  with  $P_i \in \mathcal{P}$  for  $i \in [1, m]$  and  $P_d := \{d_1, \dots, d_n\}$  stands for the set of directions in the pattern  $P \in \mathcal{P}$ , Equation (3), with  $d_j \in [1, D]$  for  $j \in [1, n]$ . Choosing  $C'$  instead of  $L_k(C')$  in the summation has no effect on  $p_k^{v,P}(\nu | i, C')$  and thus  $|C'\rangle_{\sigma_k}$ .

In iteration  $k$ , only the qubits in  $\mathcal{Q}_{k-1}^+$  with  $\mathcal{Q}_k^+ := \{q | q = q_k^i \in \mathcal{Q}_{\sigma_k} \forall i \in [1, q] \wedge \sigma_k \in L_k^+\}$  are affected by  $U^{\text{ctrl}}(C')$  for some  $C' \in \mathcal{C}_\sigma(k)$ , where  $L_k^+ := \{s | \exists C' \in \mathcal{C}_\sigma(k) : s \in S^+(L_k(C'))\}$  denotes the affected segments for  $k = [1, M]$ . Here,  $\mathcal{Q}_k^+ \subseteq \{\mathcal{Q}_1, \dots, \mathcal{Q}_k\}$  and  $L_k^+ \subseteq \{\sigma_1, \dots, \sigma_k\}$ , respectively.

The second operator in Equation (11) is the neutral operator

$$U_k^0 = \sum_{C' \in C_\sigma(k)} \left[ U_k^{\text{ctrl}}(C') \otimes U_k^{\text{init},0} + U_k^{\text{ctrl},0}(C') \right]. \quad (13)$$

Initially, all qubits  $\mathcal{Q}_k$  are in the ground state. Therefore,  $U_k^{\text{init},0} := \sum_{v \in [2, W]} |v-1\rangle \langle v-1|_{\sigma_k} \in \mathcal{H}_{\sigma_k}$  vanishes. Furthermore,  $U_k^{\text{ctrl},0}(C') := \left[ \bigotimes_{l=1}^{k-1} \mathbb{1}_{\sigma_l} - U_k^{\text{ctrl}}(C') \right] \otimes \mathbb{1}_{\sigma_k} \in \bigotimes_{l=1}^k \mathcal{H}_{\sigma_l}$  does not change the state by construction.

To realize  $U_k$  with quantum gates for a given  $k \in [1, M]$ , only  $U_k^{\text{coin}}$  has to be considered (because all other parts of  $U_k$  have no effect on the resulting state), which consists of a sequence of joint pairs  $U_k^{\text{ctrl}}(C') \otimes U_k^{\text{init}}(C')$ , one for each  $C' \in C_\sigma(k)$ . Each of these joint pairs represent a conditional loading of a probability distribution to realize  $|C'\rangle_{\sigma_k}$ , which is a well-known task that may, however, require an exponential number of gates [23].

In the original WFC, a pattern conflict leads to a restart of the algorithm. This can also be realized in QWFC by adding an additional “conflict detection qubit” that stores this information, making S1, S2, V1, and V2 obsolete. This optional extension is not further discussed.

### Technical Details of HWFC

Presume  $H$  partitions such that partition  $h \in [1, H]$  contains all of the segment identifiers from the set  $S^h \subset [1, N]$  with  $\bigcup_{h=1}^H S^h = [1, N]$  and  $\bigcap_{h=1}^H S^h = \{\}$ . The already sampled sub-contents  $C^1, \dots, C^{h-1}$  are used as an additional constraint, which has to be taken account in the quantum circuit by replacing  $C_\sigma(k)$  in Equations (12) and (13) with  $C_\sigma^h(k) := \{C \mid C = \bigcup_{i=1}^{h-1} C^i \cup C' \forall C' \in C_\sigma(k)\}$ .

### ACKNOWLEDGMENTS

Parts of this research have been funded by the Ministry of Science and Health of the State of Rhineland-Palatinate (Germany) as part of the project *AnQuC*.

### REFERENCES

1. Maxim Gumin. WaveFunctionCollapse. <https://github.com/mxgmn/WaveFunctionCollapse> [Online], 2016. Accessed on 29 July 2024.
2. Isaac Karth and Adam M. Smith. Wave function collapse is constraint solving in the wild. In *Proceedings of the 12th International Conference on the Foundations of Digital Games*, FDG '17, New York, NY, USA, 2017. Association for Computing Machinery.
3. Isaac Karth and Adam M. Smith. Wavefunctioncollapse: Content generation via constraint solving and machine learning. *IEEE Transactions on Games*, 14(3):364–376, 2022.
4. Yuhe Nie, Shaoming Zheng, Zhan Zhuang, and Julian Togelius. Nested wave function collapse enables large-scale content generation. *IEEE Transactions on Games*, pages 1–11, 2024.
5. Manabendra Nath Bera, Antonio Acín, Marek Kuś, Morgan W Mitchell, and Maciej Lewenstein. Randomness in quantum mechanics: philosophy, physics and technology. *Reports on Progress in Physics*, 80(12):124001, 11 2017.
6. Vaisakh Mannalatha, Sandeep Mishra, and Anirban Pathak. A comprehensive review of quantum random number generators: concepts, classification and the origin of randomness. *Quantum Information Processing*, 22(12), 12 2023.
7. John Preskill. Quantum Computing in the NISQ era and beyond. *Quantum*, 2:79, August 2018.
8. Michael A. Nielsen and Isaac L. Chuang. *Quantum Computation and Quantum Information: 10th Anniversary Edition*. Cambridge University Press, 2010.
9. Xinyu Mao, Wanli Yu, Kazunori D Yamada, and Michael R. Zielewski. Procedural content generation via generative artificial intelligence. *arXiv:2407.09013 [cs.AI]*, 2024. Preprint.
10. Michael Beukman, Christopher W Cleghorn, and Steven James. Procedural content generation using neuroevolution and novelty search for diverse video game levels. In *Proceedings of the Genetic and Evolutionary Computation Conference*, GECCO '22, pages 1028–1037, New York, NY, USA, 2022. Association for Computing Machinery.
11. Mar Zamorano, Carlos Cetina, and Federica Sarro. The quest for content: A survey of search-based procedural content generation for video games. *arXiv:2311.04710 [cs.SE]*, 2023. Preprint.
12. Hwanhee Kim, Seongtaek Lee, Hyundong Lee, Teasung Hahn, and Shinjin Kang. Automatic generation of game content using a graph-based wave function collapse algorithm. In *2019 IEEE Conference on Games (CoG)*, pages 1–4, 2019.
13. Arunpreet Sandhu, Zeyuan Chen, and Joshua McCoy. Enhancing wave function collapse with design-level constraints. In *Proceedings of the 14th International Conference on the Founda-*

- tions of Digital Games*, FDG '19, New York, NY, USA, 2019. Association for Computing Machinery.
14. Thijmen Stefanus Leendert Langendam and Rafael Bidarra. miwfc - designer empowerment through mixed-initiative wave function collapse. In *Proceedings of the 17th International Conference on the Foundations of Digital Games*, FDG '22, New York, NY, USA, 2022. Association for Computing Machinery.
  15. Shaad Alaka and Rafael Bidarra. Hierarchical semantic wave function collapse. In *Proceedings of the 18th International Conference on the Foundations of Digital Games*, FDG '23, New York, NY, USA, 2023. Association for Computing Machinery.
  16. Michael Beukman, Branden Ingram, Ireton Liu, and Benjamin Rosman. Hierarchical wave function collapse. *Proceedings of the AAAI Conference on Artificial Intelligence and Interactive Digital Entertainment*, 19(1):23–33, 10 2023.
  17. Yash Punia, Priyanka, and T.P Sharma. Enhancing wave function collapse algorithm using bitwise operations. In *2023 International Conference on Computer, Electronics & Electrical Engineering & their Applications (IC2E3)*, pages 1–5, 2023.
  18. James R. Wootton. Procedural generation using quantum computation. In *International Conference on the Foundations of Digital Games*, FDG'20. ACM, September 2020.
  19. James Wootton and Marcel Pfaffhauser. Investigating the usefulness of quantum blur. *arXiv:2112.01646 [cs.CV]*, 2023. Preprint.
  20. James R. Wootton. A quantum procedure for map generation. In *2020 IEEE Conference on Games (CoG)*. IEEE, 8 2020.
  21. Laura J. Piispanen. Designing quantum games and quantum art for exploring quantum physics. In *2023 IEEE Conference on Games (CoG)*, pages 1–8, 2023.
  22. Raoul Heese. Quantum Wave Function Collapse. <https://github.com/RaoulHeese/QWFC> [Online], 2023. Accessed on 29 July 2024.
  23. Kalyan Dasgupta and Binoy Paine. Loading probability distributions in a quantum circuit. *arXiv:2208.13372 [quant-ph]*, 2022. Preprint.
  24. IBM. IBM Quantum. <https://quantum.ibm.com> [Online], 2021. Accessed on 29 July 2024.
  25. RottingPixels. 2D Four Seasons Platformer Tileset [16x16]. [https://opengameart.org/content/2d-four-seasons-platformer-tileset-](https://opengameart.org/content/2d-four-seasons-platformer-tileset-16x16)
- 16x16 [Online], 2019. Accessed on 29 July 2024.